*Published version available at: https://doi.org/10.1016/j.proci.2018.06.153*

# Thermal expansion effect on the propagation of premixed flames in narrow channels of circular cross-section: multiplicity of solutions, axisymmetry and non-axisymmetry

Anne Dejoan*, Vadim N. Kurdyumov

*Department of Energy, CIEMAT. Avda. Complutense 40, 28040 Madrid, Spain*

**Abstract**

The present study examines, in presence of thermal expansion effects, the existence of the multiplicity of solutions previously reported within the context of diffusive-thermal modeling in [15], for lean premixed flames with low Lewis number ($Le < 1$) propagating in narrow circular adiabatic channels subject to a Poiseuille flow. For this, direct numerical simulations have been carried out within the framework of variable-density Navier-Stokes equations and zero-Mach-number approximation. The simulations, conducted for both axisymmetric and three-dimensional cylindrical geometries, confirm the coexistence of multiple steady flame structures for a given flow rate. They show that axisymmetric flames concave towards the upstream are more unstable to three-dimensional perturbations than convex (toward the upstream) flames. This result evinces earlier findings obtained from stability analysis. The non-axisymmetry property of the flame is also found to push back the critical flashback limits at larger flow rate when compared to those predicted under the assumption of flame axisymmetry.

*Keywords:* premixed laminar flame propagation, non-axisymmetry, three-dimensional simulations, flashback

## 1. Introduction

New technology research for the development of micro combustion devices as power source for portable devices [1–3] has promoted the interest on the problem of small-scale flame dynamics. The consequent large surface-to-volume ratio makes difficult the flame stabilization, challenging the progress in the fabrication of such small-scale combustors. Flashback, ignition and flammability limits are fundamental issues for the advancement of these innovative applications.

The propagation of premixed flame in a tube constitutes a basic configuration in the buildup of miniaturized combustors. Experiments [4–9] have shown that the characteristics of the flame propagation regime are sensitive to various

*Corresponding author:
*Email address:* anne.dejoan@ciemat.es (Anne Dejoan)

parameters such as transport, thermodynamics and conductive properties, composition mixture and tube geometry. The major difficulties encountered in the experiments are the quenching phenomena (that limits the narrowness of the tube), and the requirement of complicated techniques to maintain and control the flame, and of very small-scale measurements techniques. These drawbacks restrain a detailed description of small-scale flame characteristics.

Within the context of numerical simulation, premixed flames dynamics in a planar channel have been the focus of many studies. Simplified approaches making use of diffusive-thermal (constant density) modeling [10–14] have provided relevant effects of channel height, conductive wall properties, inlet flow rate, and of diffusion and chemical properties on the flame structure. The premixed flame propagation in planar channel has also been examined within the framework of compressible Navier-Stokes equations, accounting for simple [16, 17, 34, 35] and complex chemistry [18–20]. Besides, propagation of premixed-flame in cylindrical tubes was studied in [15, 21, 22, 24] making use of diffusive-thermal model, and in [23, 25–29, 31, 33] accounting for thermal expansion.

One pertinent question in performing numerical simulations concerns the geometry setup regarding the symmetry properties of the flame. Indeed, many of numerical studies make use of the symmetry/axisymmetry assumption for the flame shape. However, breaking of symmetry can occur as observed in some experiments [4, 6, 7]. The asymmetrical behavior of premixed flames in a planar channel have been examined in recent numerical simulations [12–14, 19, 20]. These studies outline the steady propagation of asymmetric flames in narrow channels under adiabatic/isotherm wall conditions, generally for large flow rate and Lewis numbers less or equal to unity.

Analysis of breaking of flame symmetry in cylindrical tubes is much more constraining as three-dimensionality of the geometry has to be accounted for in the simulations, thus requiring higher computational resources. These numerical limitations often promote the use of axisymmetry assumption in the simulation of flame propagating in circular channel [23, 25–30]. However, the stability analysis [15, 36] predict that loss of flame shape axisymmetry can occur under three-dimensional perturbations. Even though three-dimensional numerical results are generally scarce in the scientific literature, they do report breaking of axisymmetry of propagating flame in circular tubes with isothermal [31, 33] and adiabatic [15] wall conditions.

An interesting finding by [15] is the coexistence, for the same set of parameters, of multiple steady solutions (composed of axisymmetric and non-axisymmetric flame shapes) reported for flames with Lewis numbers smaller than unity propagating in narrow cylindrical adiabatic channels. The adiabatic wall condition falls more within a fundamental than practical purpose, nevertheless the complex flame dynamics reported in [15] under such condition is worth to be further scrutinized. Here, we propose to examine the thermal expansion effects on the multiplicity of the steady flame progation regimes. For this, variable-density numerical simulations are carried out within the zero-Mach number approximation. Identically to [15], the dynamics of the flame is examined for flames characterized by a Lewis

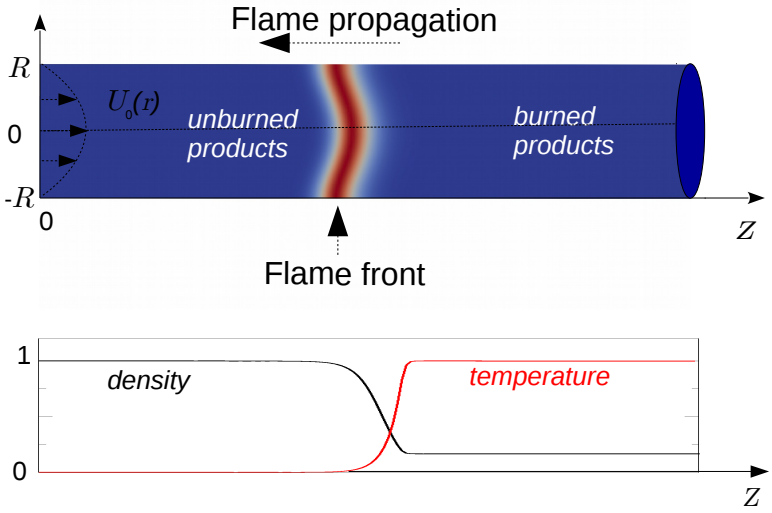


Figure 1: Sketch of the flow configuration. Flame front visualised by isocontours of reaction rate (top) and corresponding non-dimensional density and temperature profiles along the axial direction (bottom).

number less than unity. The simulations are conducted for both axisymmetrical and three-dimensional geometries.

## 2. General formulation

A combustible mixture at initial temperature $T_0$ and density $\rho_0$ flows in a channel of circular cross-section of radius $R'$. The mass flow rate at the inlet of the channel is an imposed parameter that determines the mean flow velocity in the fresh mixture. A sketch of the flow is given in Fig. 1. In all flow configurations pictured below, the fresh cold mixture is located at the left of the flame (at $z = 0$). The inlet flow may be either directed to the right when the flow rate is defined positive, as shown in Fig. 1, or to the left when the inlet flow rate is defined as negative. Depending on the flame and flow parameters, the flame front can propagate in both directions relative to the wall.

The chemistry is modeled by a global, one step and irreversible reaction of the form $F + O \rightarrow P + Q$, where $F$, $O$ and $P$ denote the fuel, the oxidizer and the products, respectively, and $Q$ is the heat released per unit mass of fuel. We assume for simplicity that the mixture is lean in fuel and consider the oxidizer mass fraction as constant. Then, the reaction proceeds at the rate $\Omega = \mathcal{B}\rho'^2 Y' \exp(-E/\mathcal{R}T)$, where $E$ is the overall activation energy, $\mathcal{R}$ is the universal gas constant, $Y'$ is the fuel mass fraction and $\mathcal{B}$ is a pre-exponential factor containing the oxidizer mass fraction.

The burning velocity of the planar flame, $S_L$, the thermal flame thickness defined as $\delta_T = \mathcal{D}_T/S_L$, together with the adiabatic flame temperature $T_a = T_0 + QY_0/c_p$ are used below to specify the non-dimensional parameters. In the

above expressions, $\mathcal{D}_\mathcal{T}$ stands for the thermal diffusivity, $c_p$ for the specific heat at constant pressure and $Y_0$ for the upstream fuel mass fraction. In what followed the constant transport properties and the specific heat are assumed.

The appropriate dimensionless variables are $(z, r) = (z', r')/\delta_T$, $t = S_L t'/\delta_T$, $\mathbf{v} = \mathbf{v}'/S_L$, $\rho = \rho'/\rho_0$, $p = p'/\rho_0 S_L^2$, $\theta = (T - T_0)/(T_a - T_0)$ and $Y = Y'/Y_0$, where primes are used for the corresponding dimensional variables. Here $p'$ is the pressure deviation from the ambient (atmospheric) pressure which, in view of the low Mach number approximation adopted here, is constant. The non-dimensional channel's radius writes as $R = R'/\delta_T$ and the reduced Damköhler number used below is defined by $d = (R'/\delta_T)^2 = R^2$.

The standard (dimensionless) governing equations become

$$\rho_t + \nabla \cdot (\rho \mathbf{v}) = 0, \tag{1}$$

$$\rho \mathbf{v}_t + \nabla \cdot (\rho \mathbf{v} \cdot \mathbf{v}) = -\nabla p + Pr \nabla (\nabla \cdot \mathbf{v} + \nabla \cdot \mathbf{v}^T), \tag{2}$$

$$\rho \theta_t + \nabla \cdot (\rho \theta \mathbf{v}) = \nabla^2 \theta + \omega, \tag{3}$$

$$\rho Y_t + \nabla \cdot (\rho Y \mathbf{v}) = Le^{-1} \nabla^2 Y - \omega, \tag{4}$$

$$\rho (1 + q\theta) = 1, \tag{5}$$

where subscripts here and below denote partial differentiation.

The dimensionless parameters appearing in Eqs. (1)-(5) are the heat release parameter $q = (T_a - T_0)/T_0$, the Lewis number $Le = \mathcal{D}_T/\mathcal{D}_F$, where $\mathcal{D}_F$ stands for the molecular diffusivity of the fuel, and the Prandtl number $Pr = \nu/\mathcal{D}_T$, where $\nu$ is the kinematic viscosity of the mixture. The dimensionless reaction rate $\omega = \Omega \mathcal{D}_T/\rho_0 S_L^2 Y_0$ is given by:

$$\omega = \frac{\beta^2}{2 Le u_p^2} (1 + q)^2 \rho^2 Y \exp\left\{ \frac{\beta(\theta - 1)}{(1 + q\theta)/(1 + q)} \right\}, \tag{6}$$

where $\beta = E(T_a - T_0)/\mathcal{R} T_a^2$ represents the Zel'dovich number. The factor $u_p = S_L/U_L$ appearing in Eq. (6) is introduced to account for the difference between the assymptotic value of the laminar flame speed obtained for large activation energy $\beta \gg 1$, $U_L = \sqrt{2 Le \beta^{-2} \mathcal{D}_T \mathcal{B} \rho_0}\ (T_0/T_a)\, \mathrm{e}^{-E/2\mathcal{R}T_a}$. The factor $u_p$ ensures that for a given $\beta$ the non-dimensional speed of a planar flames equals to one. In what followed we use $\beta = 10$, $q = 5$ as representative values. The corresponding numerical values of $u_p$ calculated for $Le = 0.7$ and 0.5 are 1.0851 and 1.1068, respectively.

Equations (1)-(5) are solved subject to the following boundary conditions: at the inlet of the pipe (in the fresh mixture), the velocity field corresponds to a fully developed Poiseuille flow with the given dimensionless flow rate $m$; at the outlet of the pipe, the velocity, temperature, density and mass fraction satisfy zero-gradient boundary condition;

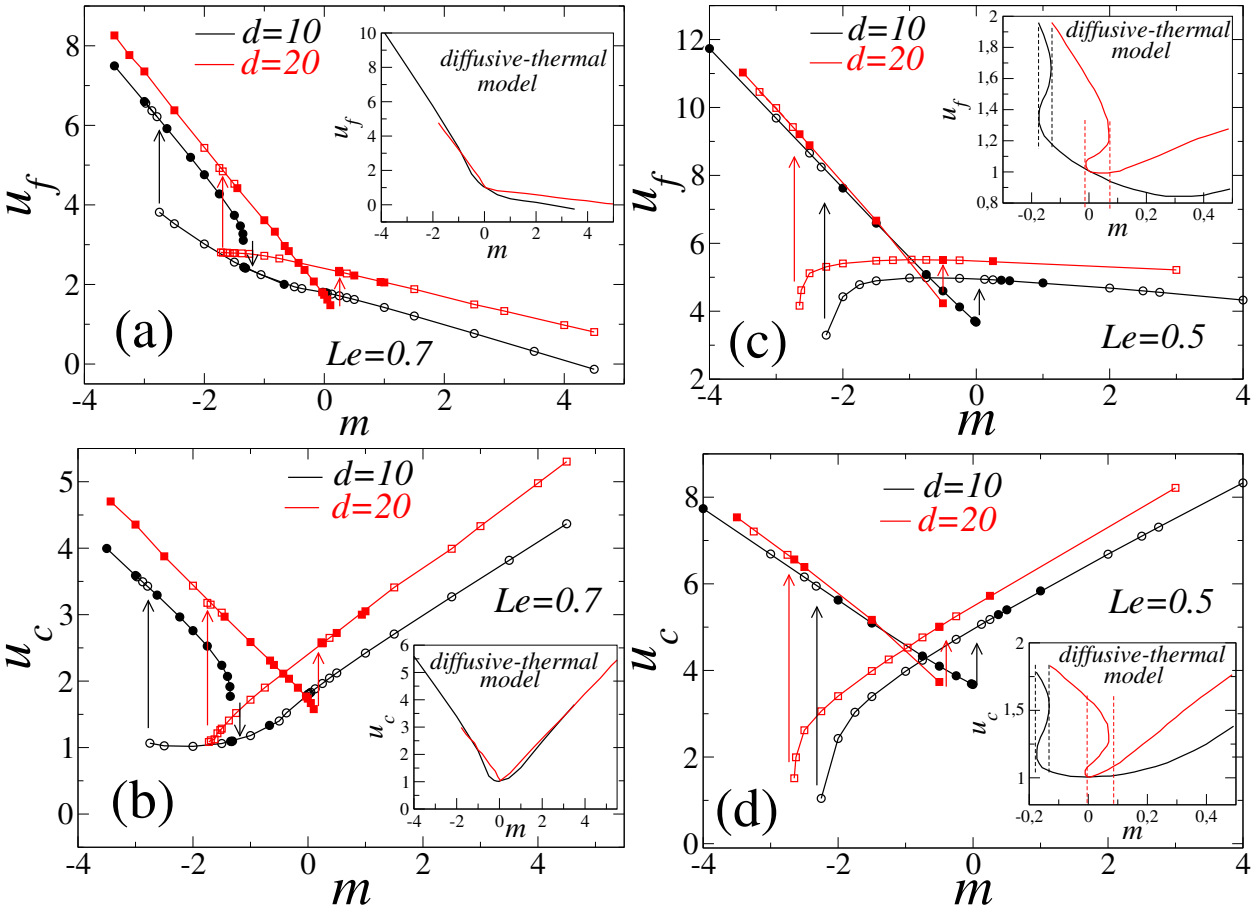


Figure 2: Axisymmetric solutions; flame velocity $u_f$ and consumption speed $u_c$ given as a function of the flow rate $m$ for $d = 10$ and $d = 20$ for $Le = 0.7$ ((a) and (b)) and $Le = 0.5$ ((c) and (d)). Arrows delimit the region of solution multiplicity. In the inset plots results obtained within the frame of thermo-diffusive modeling by [15] are recalled and the corresponding regions of solution multiplicity are delimited by dashed lines.

the wall is considered as non-slip and adiabatic.

The selected reference frame moves with the flame. This is achieved by an iterative correction of the axial flow velocity (see [19]) aimed to balance $m$ with the velocity consumption $u_c$, whose dimensionless expression is given by $u_c = 1/(\pi R^2) \int_{-\infty}^{+\infty} \int_0^R \int_0^{2\pi} \omega d\varphi dr dz$. Once the balance is reached, the wall moves with respect to the wall at the dimensionless velocity given by $u_f = u_c - m$, and the flame position is fixed inside the computational domain. A stationary solution, by reference to the moving system, is thus obtained. It should be noted that, in all cases considered below, $Le < 1$ and the flame propagated with a constant velocity.

The set of dimensionless equations (1)-(5) was resolved for both the axisymmetric and fully three-dimensional computations making use of as a baseline the open source Computational Fluid Dynamics (CFD) code OpenFoam [37]. In the axisymmetric simulations, the standard axisymmetry boundary conditions used at the pipe axis. The three-dimensional computational domain consists of a triangular prism decomposition with computational cells of almost-

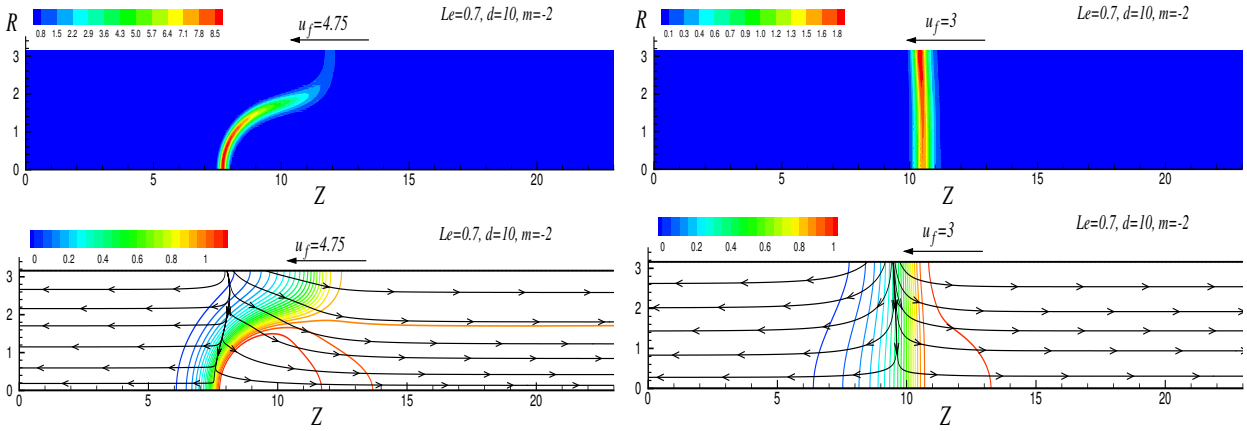


Figure 3: Axisymmetric pipe: multiple solutions; $d = 10$, $Le = 0.7$, $m = -2$; visualization of (top) reaction rate isocontours and (bottom) streamlines superimposed with isocontours of temperature $\theta$;

uniform size, having their base distributed orthogonally to the axial direction (O$z$). The implemented numerical method is based on the finite volume method formulated in a collocated grid arrangement. The first order Euler scheme was used for temporal discretization and second-order scheme for spatial discretization. In the axisymmetric simulations the grid-resolution takes the dimensionless values $\delta_r = 0.1$ and 0.05 for $Le = 0.7$ and $Le = 0.5$, respectively. Grid independance of the steady converged solutions was checked by performing simulations with half grid resolution that provide results with less than 2% of difference. A total cell number of 1773360 has been used to discretize the three-dimensional pipe computational domain in each simulation presented. Grid resolution identical to the axisymmetric simulations was used for $Le = 0.7$ while it was slightly relaxed to 0.07 for $Le = 0.5$. The time step required to maintain numerical stability and ensure convergence of the solution is close to $5 \times 10^{-5}$ in dimensionless unit. The converged stationary solution is obtained after a transient time, once the balance between consumption speed and flow rate is reached and the velocity flame propagation becomes constant. It is important to note that, as consequence of the time-marching procedure used in the present computations, the steady solutions obtained here are stable. Finally, the control parameters selected here for the analysis of the flame dynamics are the inlet flow rate $m$, the Lewis number $Le$ and the Damköhler number $d$ (or, equivalently, the pipe radius).

## 3. Axisymmetric simulations

The evolution of the flame propagation velocity, $u_f$, and of the burning velocity, $u_c$, are given as a function of the inlet flow rate $m$ for the Lewis number $Le = 0.7$ and 0.5, in Fig. 2 (a)-(b) and Fig. 2 (c)-(d), respectively, for the two Damköhler numbers $d = 10$ and 20. It is shown that, over a range of flow rate, a region of multiple solutions exists, in agreement with the diffusive-thermal modeling-based simulations [15]. However, by comparison with the predictions provided by the diffusive-thermal approach, recalled in the inset plots of Fig. 2, the occurrence of multiple solutions

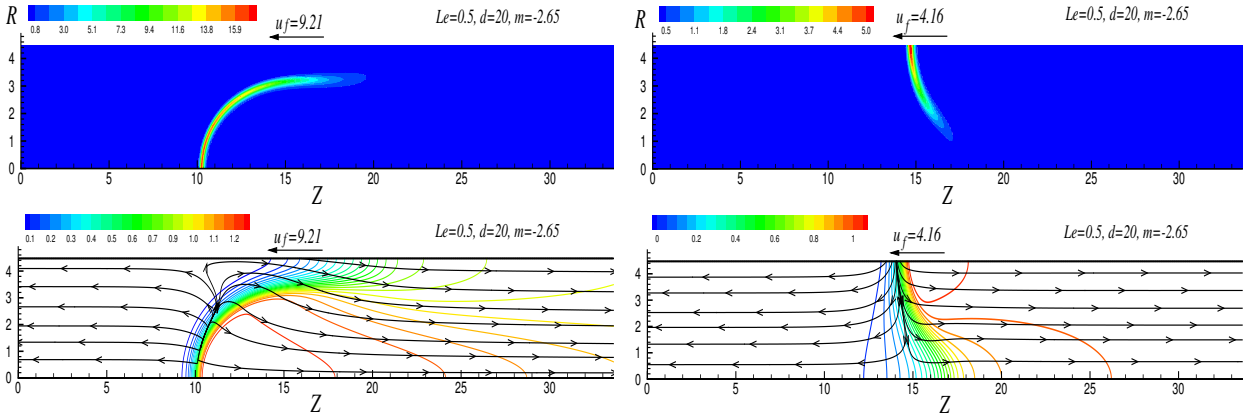


Figure 4: Axisymmetric pipe; multiple solutions: $d = 20$, $Le = 0.5$, $m = -2.65$; visualization of (top) reaction rate isocontours and (bottom) streamlines superimposed with isocontours o

is displaced from near zero to negative values of $m$ when thermal expansion is accounted for. Moreover, multiplicity of solutions appears for larger values of $Le$. Indeed, for identical parameters as those considered here, multiplicity in [15] is only found for $Le = 0.5$.

The shift of multiplicity region to negative values of $m$ can be explained by the effect of the net flow on the flame curvature, that results from both the axial velocities upstream (imposed Poiseuille velocity at the pipe inlet) and downstream (increase of axial velocity due to mass continuity) of the flame front. When thermal expansion is not included, the flame curvature is mainly governed by the fluid velocity imposed at the inlet pipe. As for example, right Fig. 3 ($Le = 0.7$, $m = -2$ and $u_f = 3$) illustrates the case where the reverse flow direction through the front flame has an opposit effect to the negative imposed inlet pipe velocity on the flame curvature, resulting in an almost planar flame front. By reference to the non-dimensional parameters, the planar flame occurs for $m = 0$ in the diffusive-thermal approach by [15]. The increase of axial velocity modifies the flame curvature and thus the flame dynamics when compared to the diffusive-thermal modeling.

Figure 3 displays the flame and flow structures for the case $Le = 0.7$, $d = 10$ and $m = -2$, for which multiple solutions are found. In this case, the upper branch of the solution corresponds to a convex flame towards the inflow with a overheated region located close to the pipe axis, similar to a mushroom-shaped flame. Otherwise, the lower branch coincides with a flame having a overheated region located near the pipe wall and resembling a tulip-shaped flame. In this case, the former flame structure presents the highest curvature and thus the larger flame propagation.

Shown in Fig. 2 is the crossing of the mushroom-shaped and tulip-shaped flame branches as $d$ increases ($d = 20$ and $Le = 0.7$) or $Le$ diminishes ($d = 10$ and 20, $Le = 0.5$). Before crossing, the flame characteristics illustrated in Fig. 4 for $Le = 0.5$, $d = 20$ and $m = -2.65$ are similar to those reported above for $Le = 0.7$, $d = 10$ and $m = -2$. Above crossing, as $m$ increases, a reverse tendency is observed: the mushroom-shaped flame branch has a smaller

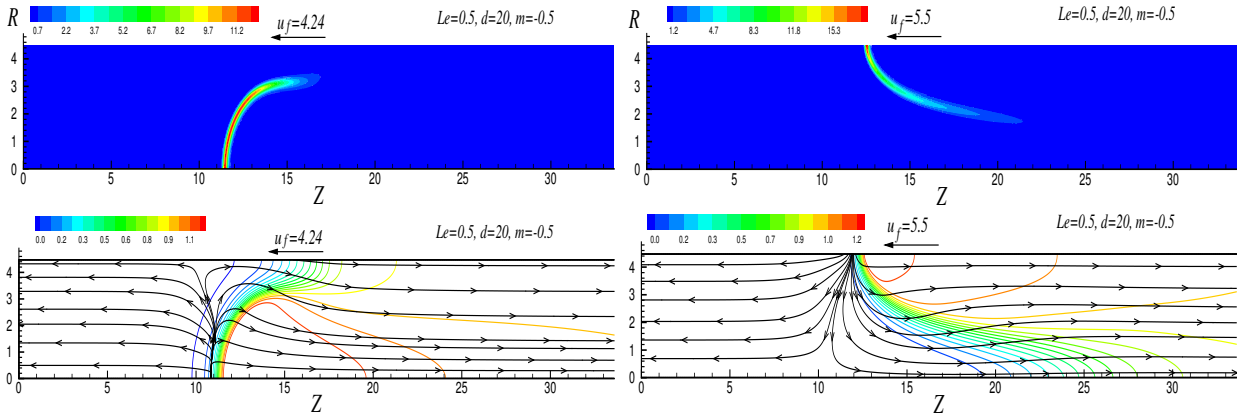


Figure 5: Axisymmetric pipe; multiple solutions: $d = 20$, $Le = 0.5$, $m = -0.5$; visualization of (top) reaction rate isocontours and (bottom) streamlines superimposed with isocontours of temperature $\theta$;

curvature and thus a lower propagation velocity than the tulip-shaped flame branch. This behavior is pictured in Fig. 5 for $Le = 0.5$, $d = 20$ and $m = -0.5$. Note that coexistence of mushroom and tulip premixed-flames with Lewis number unity, freely propagating in axisymmetric tubes, has been reported in the early numerical study by [25], under adiabatic and isotherm wall conditions, and radius $R \geq 60$.

The streamlines drawn in Figs. 3-5 clearly show the jump of the axial velocity through the flame front resulting from thermal expansion previously mentioned above. Contrary to the diffusive-thermal modeling approach, the curvature of the flame is subject to the flow acceleration through the front flame which in turn alters the consumption speed and flame velocity propagation. The differences in terms of parameters ($Le$, $d$ and $m$) at which multiple solutions are observed here, when compared with [15], result from the effect of thermal expansion on the flame curvature. Note that, in the present simulations, it is not possible to fix the flame propagation velocity and compute the corresponding inlet flow rate to make the two flame branches continuously recover as done in [15].

## 4. Three-dimensional simulations

Figures 6 (a)-(b) provide a direct comparison between the three-dimensional and axisymmetric simulation results of the evolution of $u_f$ and $u_c$ as a function of the flow rate $m$, for $Le = 0.7$ and $d = 10$. Similar to the axisymmetric calculations, only steady and stable solutions have been obtained. The evolution of $u_f$ and $u_c$ show that, for large negative values of the inlet flow rate ($m < -3$), the three-dimensional simulations display a unique axisymmetric propagating flame, while as $m$ is increased, axisymmetric and non-axisymmetric steady-state flame regimes can coexist. However, for $m \geq -1$ the three-dimensional simulations predict a unique non-axisymmetric propagating flame. For large positive flow rates $m \geq 9$, the flame reverses its propagation direction and flashback occurs. Note that, identically to the results reported for a planar channel in [19], the non-symmetric flame propagation regime pushes back the flashback

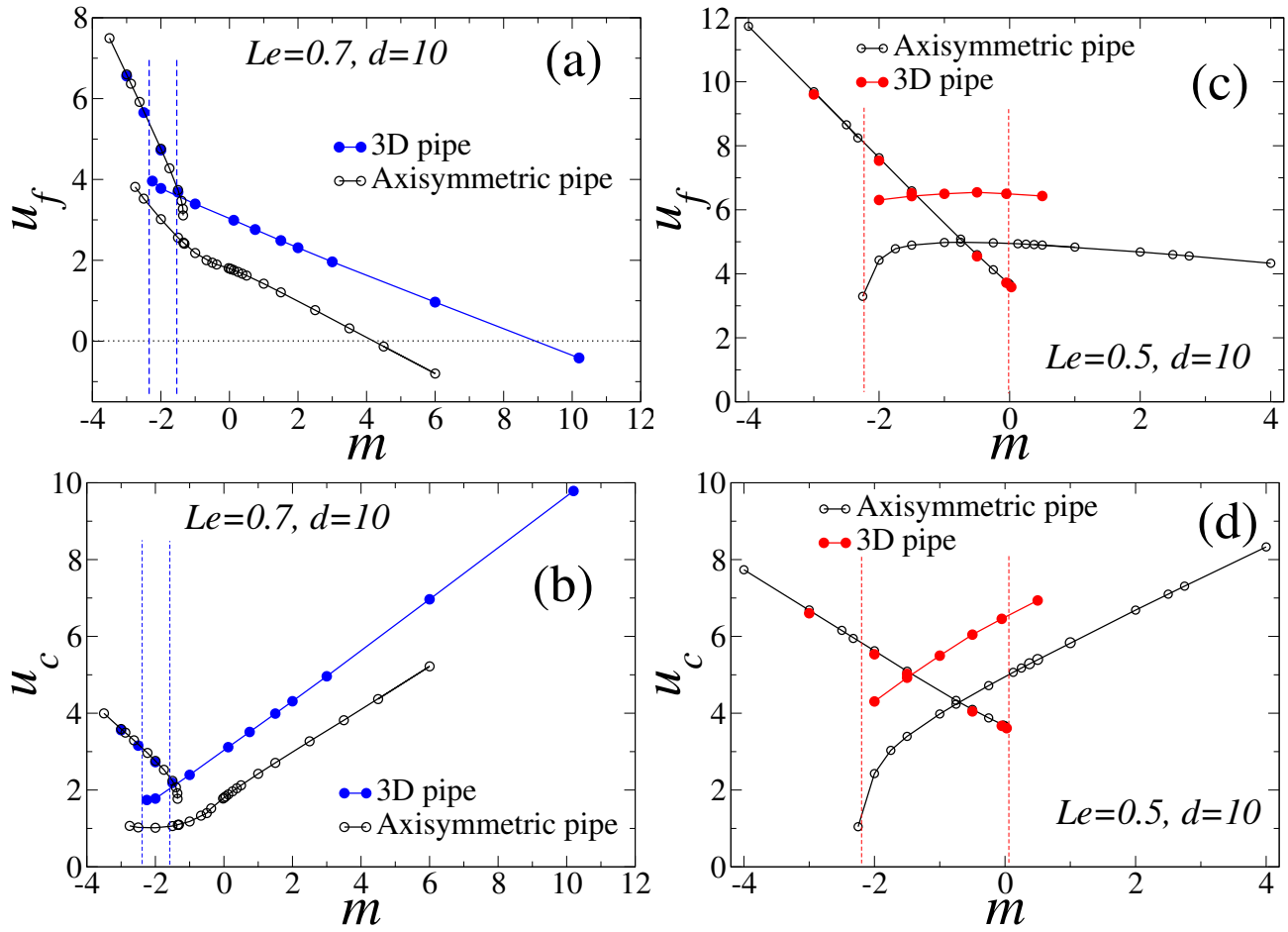


Figure 6: 3D solutions; flame velocity $u_f$ (top) and consumption speed, $u_c$ (bottom), as a function of the dimensionless flow rate $m$, obtained for $d = 10$ with $Le = 0.7$ and 0.5. Dashed lines delimit the region of solution multiplicity for the 3D simulations.

phenomena to larger $m$ ($m \sim 9$) when compared with the predictions of the corresponding axisymmetric calculations ($m \sim 4$).

Due to computational limitations, the simulations for $Le = 0.5$ have been restricted to a few values of $m$. Nevertheless, the main characteristics in terms of axisymmetry and non-axisymmetry of the flame shape, are similar to those found for $Le = 0.7$. In this case, the two solution branches cross, the coexistence of axisymmetric and non-axisymetric solutions extending over a larger range of inlet flow rate values compared to $Le = 0.7$.

An overview of the evolution of the flame structure, as a function of $m$, is drawn in Fig. 7 for $Le = 0.7$, by representing the given isosurface of dimensionless temperature $\theta$=0.9 and the isocontours of the dimensionless reaction rate $\omega$ in the transversal plane $y = 0$. For $m = -3$, the axisymmetric solution has a mushroom-like shape. As $m$ is further increased, the flame becomes non-axisymmetric and is further stretched, with tulip-like flame characteristics in the transverse plane $y = 0$ and a slant-like shape in the transverse plane $x = 0$. The also pictured streamlines and

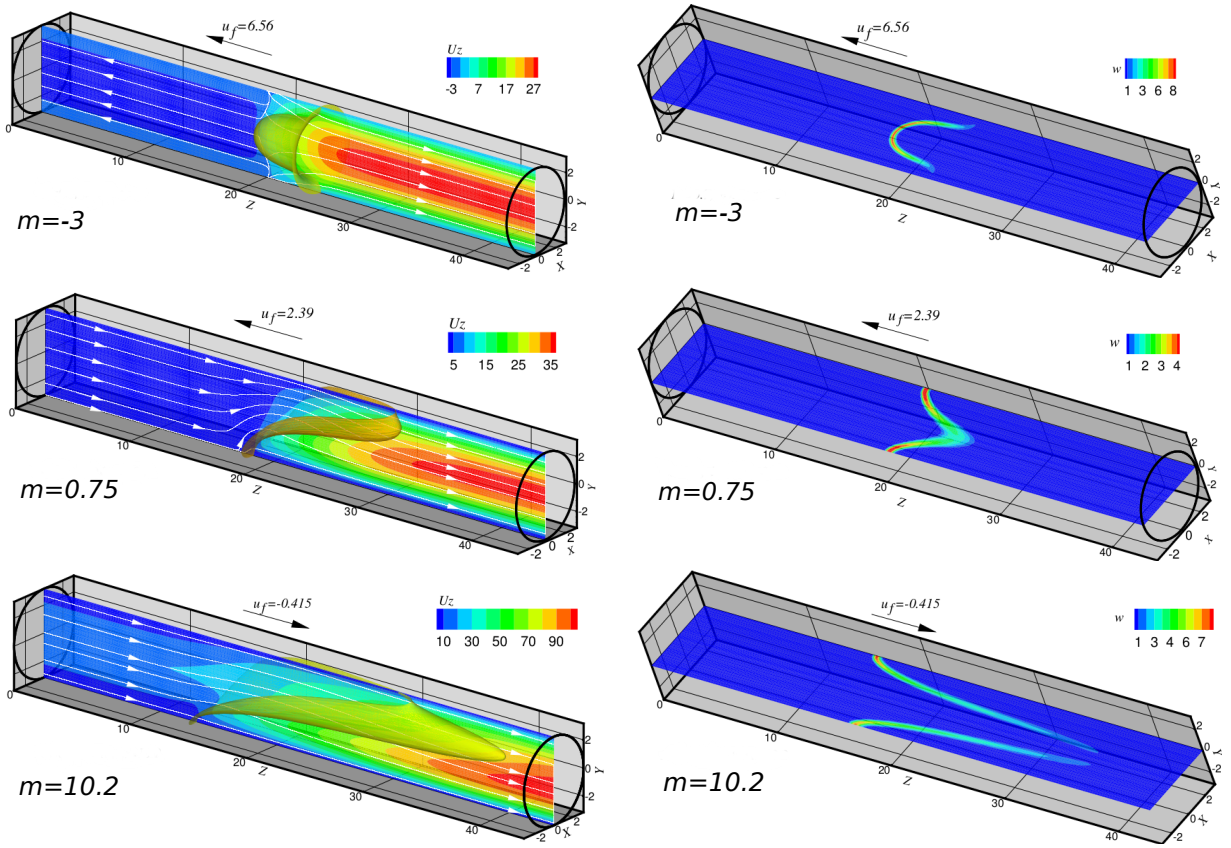


Figure 7: 3D circular pipe; $d = 10$, $Le = 0.7$; evolution of flame structure with $m$; (left): isosurface temperature $\theta = 0.9$ superimposed with the streamlines and isocontours of axial velocity both given in the plane $x = 0$; (right): isocontours of reaction rate given in the plane $y = 0$.

isocontours of the axial flow velocity $U_z$ display the manifest jump of axial velocity through the flame that can reach a factor 10 between upstream and downstream of the flame front.

The multiple flame solutions obtained for $m = -2$ in the three-dimensional pipe is represented in Fig. 8 for $Le = 0.7$, and in Fig. 9 for $Le = 0.5$. In Fig. 10 is provided the double flame structure found for $m = -0.05$ and $Le = 0.5$. In all cases, the axisymmetric flame corresponds to the mushroom-shaped flame, with the overheated region in the pipe axis, while the non-axisymmetric flame has the slant shape with the overheated region near the pipe wall. Note that, above the multiple solutions region at large values of $m$, only non-axisymmetric flames develop and that no solution corresponding to axisymmetric tulip-shaped flame have been found in the three-dimensional simulations.

These results indicate that the axisymmetric tulip-shaped flame does not remain stable to three-dimensional perturbations while the axisymmetric mushroom-shaped flame does. This result corroborates the stability analysis reported in [15]. We find that axisymmetric convex flames towards the upstream (mushroom flame) can remain stable for large negative inlet flow rate. However, the axisymmetric concave flame (tulip flame) evaluates to a non-axisymmetric flame under three-dimensional perturbations for any values of the considered parameters here.

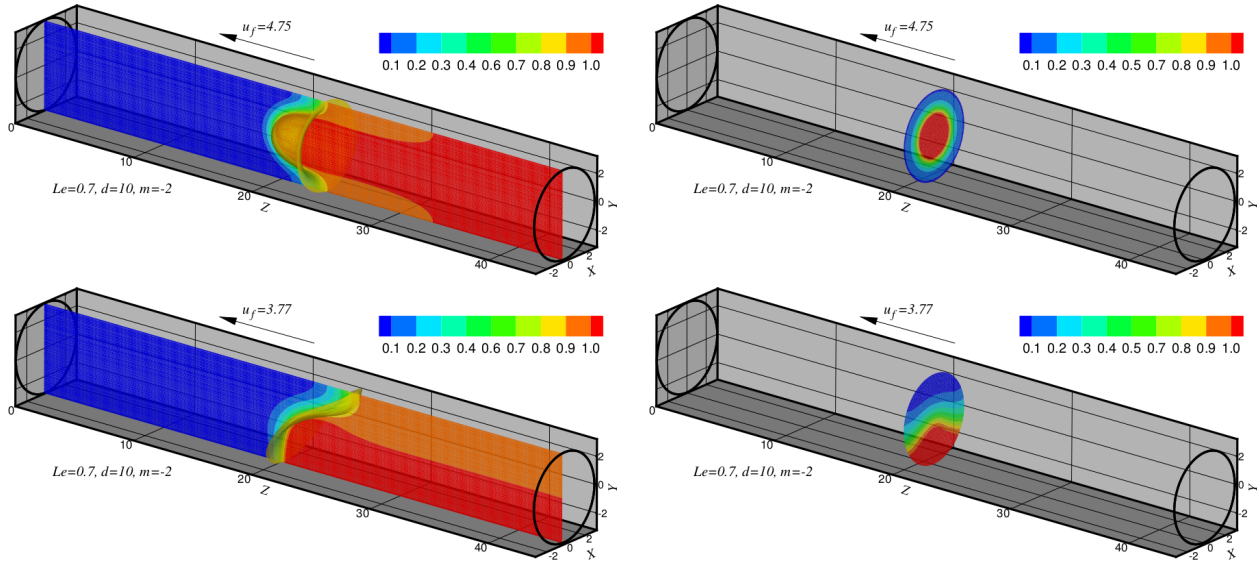


Figure 8: 3D circular pipe; multiple solutions: $d = 10$, $Le = 0.7$, $m = -2$; (left): isosurface of temperature $\theta = 0.8$ superimposed with the temperature contours given in the transversal plane $x = 0$; (right): temperature isocontours given in the radial plane $z = L_z/2$ (right).

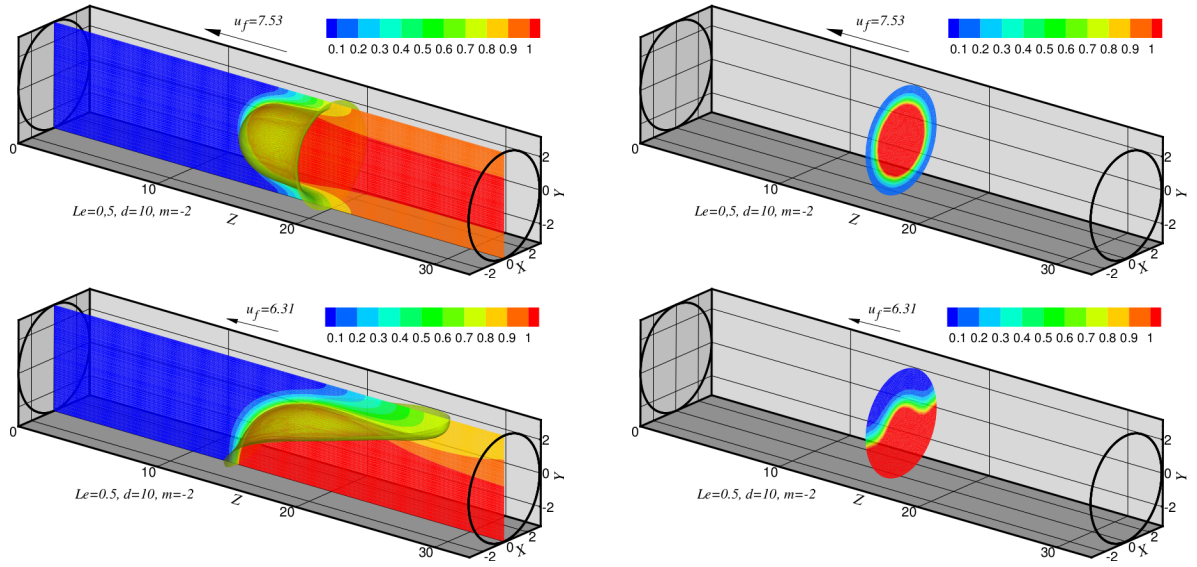


Figure 9: 3D circular pipe; multiple solutions: $d = 10$, $Le = 0.5$, $m = -2$; isosurface of temperature $\theta = 0.8$ superimposed with the temperature contours given in the transversal plane $x = 0$ (left); temperature isocontours given in the radial plane $z = L_z/2$ (right).

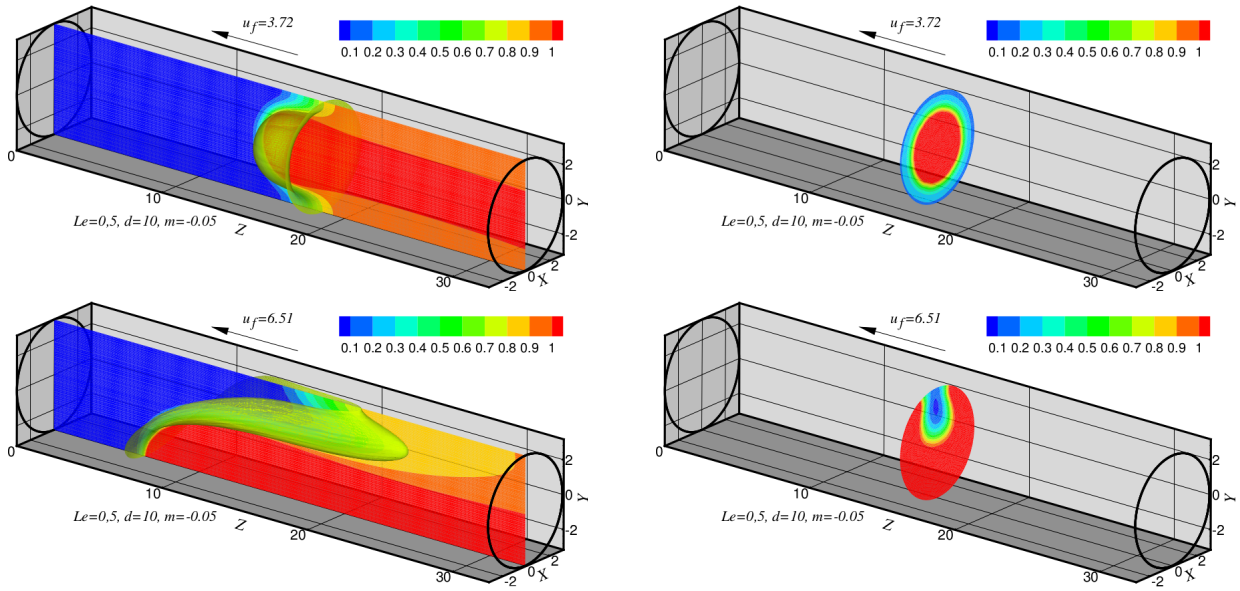


Figure 10: 3D circular pipe; multiple solutions: $d = 10$, $Le = 0.5$, $m = -0.05$; isosurface of temperature $\theta = 0.8$ superimposed with the temperature contours given in the transversal plane $x = 0$ (left); temperature isocontours given in the radial plane $z = L_z/2$ (right).

## 5. Conclusions

The propagation regime of lean premixed low-Lewis number flames in a channel of circular cross-section with imposed Poiseuille inlet flow was investigated making use of numerical simulations and simplified chemistry model. This study aimed to illustrate how far thermal expansion influences the multiplicity of solutions and breaking of axisymmetry, previously found within a diffusive-thermal modeling approach by [15]. The considered flow and flame parameters were the flow rate of the fresh mixture $m$, the Lewis number $Le$ (less than unity), and the tube radius $R$ in term of Damköhler number $d = \sqrt{R}$.

Making use of axisymmetry assumption for the pipe geometry, the present numerical simulations confirm the existence of multiple steady axisymmetric flame propagation regimes for a given flow rate: both convex and concave flames towards the upstream flow can coexist. Under thermal expansion effects, multiplicity of flame propagation regimes is shown to appear at larger (but less than unity) Lewis number in comparison with the constant density approach, as consequence of the modification of the flame structure by the flow acceleration through the front flame.

The three-dimensional simulations also show a multiplicity of solutions. However, the axisymmetric concave flame branch is not obtained, instead the steady propagation regime of non-axisymmetric flames takes place. By contrast, the branch corresponding to the axisymmetric convex flame shape remains robust for large negative values of the inlet flow rate $m$. These findings complete and point out the earlier stability analysis results [15] that predict axisymmetric concave flames are unstable under three-dimensional perturbations, giving rise to steady non-axisymmetric

flames. The present results show that the range of inlet flow rate for which axisymmetric and non-axisymmetric flames coexist tends to further extend as the Lewis number decreases.

Regarding the set up of numerical simulations, this study shows that the assumption of axisymmetry is not adequate for the numerical study of propagating flames in circular tubes, excepted in the range of large negative inlet flow rate (flame-assisted flow). Another result, of practical interest, is the underestimation of the critical flow rate for the flashback phenomena provided by the use of axisymmetry assumption.

Finally, the effects of heat wall-loss on the solution multiplicity and breaking of symmetry reported here will be the focus of a future work.

## Acknowledgments

The support of Spanish MEC under Project #ENE2015-65852-C2-2-R is gratefully acknowledged.

## References

[1] C. Fernández-Pello, Proc. Combust. Inst. 29 (2002) 883–899.

[2] D. C. Walther, J. Ahn, Prog. Energy Combust. Sci. 37 (2011) 583–610.

[3] Y. Ju, K. Maruta, Prog. Energy Combust. Sci. 37 (2011) 583–610.

[4] U. Dogwiler, J. Mantzaras, P. Benz, B. Kaeppeli, R. Bombach, A. Arnold, Proc. Combust. Inst. 27 (1998) 2275–2282.

[5] K. Maruta, T. Kataoka, N. I. Kim, S. Minaev, R. Fursenko, A. Arnold, Proc. Combust. Inst. 30 (2005) 2429–2436.

[6] V. N. Kurdyomov, E. Fernández-Tarrazo, J. M. Truffaud, J. Quinard, A. Wangher, G. Searby, Proc. Combust. Inst. 31 (1) (2007) 1275–1282.

[7] N. I. Kim, T. Kataoka, S. Maruyama, K. Maruta, Combust. Flame 141 (2005) 78–88.

[8] C. J. Evans, D. C Kyritsis, Combust. Sci. and Tech. 183 (2011) 847–867.

[9] T. A. Connely, D. C Kyritsis, J. Energy Eng. 141(2) (2015) C4014016-1-7.

[10] J. Daou, M. Matalon, Combust. Flame 124 (3) (2001) 337–349.

[11] J. Daou, M. Matalon, Combust. Flame 128 (4) (2002) 321–339.

[12] V. N. Kurdyomov, G. Pizza, C. Frouzakis, J. Mantzaras, Combust. Flame 156 (2009) 2190–2200.

[13] V. Kurdyumov, Combust. Flame 158 (7) (2011) 1307–1317.

[14] V. Kurdyumov, C. Jiménez, Combust. Flame 161 (4) (2014) 927–936.

[15] V. Kurdyumov, C. Jiménez, Combust. Flame 167 (2016) 149–163.

[16] C. L. Hackert, J. L. Elisey, A. Ezekoye, Combust. Flame 112 (1998) 73–84.

[17] M. Short, M. Kessler, J. Fluid Mech. 638 (2009) 305–317.

[18] G. Pizza, C. E. Frouzakis, J. Mantzaras, A. G. Tomboulides, K. Boulouchos, Combust. Flame 152 (2008) 433–450.

[19] C. Jiménez, D. Fernández-Galisteo, V. Kurdyumov, Int. J. Hydrogen Energy 40 (2015) 12541–12549.

[20] C. Jiménez, V. Kurdyumov, Proc. Combust. Inst. 36(1) (2017) 1559–1567.

[21] V. N. Kurdyumov, E. Fernández-Tarrazo, Combust. Flame 128 (4) (2002) 382–394.

[22] E. Barrios, J. C. Prince, C. Treviño, Combust. Theory Model. 12(1) (2007) 115–133.

[23] S. T. Lee, J. S. Tien, Combust. Flame 48 (1982) 273–285.

[24] T. L. Jackson, J. Buckmaster, Z. Lu, D: C. Kyritsis, L. Massa Proc. Combust. Inst. 31 (2007) 955–962.

[25] S. T. Lee, C. H. Tsai, Combust. Flame 99 (1994) 484–490.

[26] V. Bychkov, A. Kleev, Phys. Fluids 11 (1999) 1890–1895.

[27] J.D. Ott, E.S. Oran, J.D. Anderson, AIAA J. 41 (2003) 13911396.

[28] V.N. Gamezo, E.S. Oran, AIAA J. 44 (2006) 329 336.

[29] N. I. Kim, K. Maruta, Combust. Flame 146 (2006) 283–301.

[30] V. Bychkov, V. Akkerman, G. Fru, A. Petchenko, L-E. Eriksson Combust. Flame 150 (2007) 263-276.

[31] C.-H. Tsai, Combust. Sci. Tech. 180 (2008) 533–545.

[32] V. Akkerman, C.K. Law, V. Bychkov, L-E. Eriksson, Phys. Fluids 22 (2010) 053606

[33] G. Pizza, C. E. Frouzakis, J. Mantzaras, A. G. Tomboulides, K. Boulouchos, J. Fluid Mech. 658 (2010) 463–491.

[34] V.N. Kurdyumov, M.Matalon, Proc. Combust. Inst. 35 (2015) 921-928.

[35] V.N. Kurdyumov, M.Matalon, Proc. Combust. Inst. 36 (2017) 1549-1557.

[36] A. Petchenko, V. Bychkov, Axisymmetric versus non-axisymmetric flames in cylindrical tubes, Combust. Flame 136 (2004) 429–439.

[37] User, P. G. T. Report, http://www.openfoam.com.

**List of Figures**